In-Flight Measurement of Static Pressures and Boundary-Layer State with Integrated Sensors

E. Greff*
Messerschmitt-Bölkow-Blohm GmbH, Bremen, Germany

Advanced wing designs for transport aircraft using adaptive geometries for performance optimization and load control need reliable integrated sensors for feedback to the control system. More efficient air data sensing, eliminating the pitot-static piping, is also required, as in highly integrated modern flight management systems. Absolute pressure transducers from different manufacturers were tested and adapted to the flight-test environment. In laboratory and different flight tests, their applicability for steady measurements was proven in comparison to scanivalves. It was shown that sensing of pressure fluctuations in the buffet regime will improve the prediction of operational buffet limits. The pressure transducers were also used to investigate the laminar/turbulent transition in the attachment-line flow of a swept wing in comparison to hot-film probes and were found to be an effective tool for such an experiment.

Nomenclature

C_l = lift coefficient
C_z = uncorrected lift coefficient, $(n_Z W)/(q_\infty S)$
c = chord length
M = Mach number
n_Z = vertical load factor
p = static pressure
q = total velocity
q_∞ = dynamic pressure
R = electrical resistance
Re = Reynolds number
S = wing reference area
s = arc length
T = temperature
t = time
$U(p,T)$ = transducer output voltage
W = weight
α = angle of attack
β = angle of sideslip
ϵ = strain
η = spanwise coordinate
ν = kinematic viscosity
ϕ_{LE} = leading-edge sweep angle

Subscripts

a = ambient conditions
b = buffet
e = edge of boundary layer
∞ = freestream condition

Introduction and Basic Remarks

AIR data measurements depend greatly on the accuracy of sensed pressures and temperatures. Although accurate total pressures and temperatures can be sensed quite readily, accurate sensing of static pressures has given and continues to give problems.[1-3]

Unfortunately, static pressure is an element in the computation not only of altitude, but of airspeed, true airspeed, and Mach number. Increasing complexity of modern control systems for transport aircraft as well as military aircraft, however, requires more accurate sensing of aerodynamic parameters, because they will be used as control system feedback.[4]

In addition to aircraft performance and control aspects, sensing of local flow properties of the boundary-layer flow in full scale becomes increasingly important for aerodynamicists involved in research and design of modern transonic wings with natural laminar flow, variable camber, and turbulence management.

During the A310 flight-test program, pressure distributions were measured in several spanwise sections using scanivalves and pneumatic tubing. The results were influenced largely by tubing-related error sources and mechanical or electrical malfunction of the scanivalves. The agreement with pressure distributions on wind-tunnel models has been quite poor. That was the motivation to look for alternative pressure sensing devices. This paper concentrates mainly on the measurement of pressures with piezoresistive transducers and also reports on hot-film measurements in the vicinity of the attachment line of an A310 aircraft in a high-lift configuration.

A proof of a less expensive retrofittable and reliable system with integrated sensors could change the priorities and enable the aerodynamicist to use the flight test as a development tool more often.

Next-generation transport aircraft will use more advanced aerodynamic technologies, e.g., variable camber (VC) for the control of L/D, buffet boundary, and maneuver loads.[5,6] The integration of VC into an automatic control system leads to the concept of an "intelligent wing," which is depicted in Fig. 1. In addition to the primary inputs from the pilot, e.g., speed, altitude, and initial weight, the system sets the lift distribution close to the buffet boundary according to the measured trailing-edge pressure along the wingspan with integrated sensors. In the same manner, load control can be achieved by employing suitable strain sensors and accelerometers. The control surfaces, namely, wing flaps, spoilers, and ailerons (flaperons), will be deployed by the aircraft flight management system, giving the highest priority, however, to primary control. For such a control system, a reliable integrated pressure sensor is a prerequisite.

Feasibility of Miniature Pressure Sensors for Flight Testing

Fundamentals of Piezoresistive Transducers

Silicon integrated sensors are fabricated by using the techniques of transistor and integrated circuit manufacturing. A

Received April 29, 1989; presented as Paper 89-2209 at the AIAA 7th Applied Aerodynamics Conference, Seattle, WA, July 31-Aug. 2, 1989; revision received April 10, 1990.

*Head, Aerodynamic Design Department, Transport Aircraft Division. Member AIAA.

silicon wafer is used as a diaphragm over an evacuated cavity (Fig. 2). The piezoresistive elements are formed integral to the silicon pressure-sensitive diaphragm by solid-state diffusion. Thus, the resistors of the Wheatstone bridge are integrated into the mechanical flexure.[7]

The physical dimensions of the available sensors are on the order of a few millimeters, thus enabling surface flush mounting of the sensing device.

Several transducers from different manufacturers were investigated and checked with respect to their applicability in flight. The flight-test environment is quite different from laboratory and wind-tunnel conditions, and the sensors offered initially did not yield an acceptable accuracy. Since they are used as absolute pressure sensors to avoid sizable lengths of reference piping, the suitable pressure range is 15 psia. Scatter in pressure coefficients should be less than 0.05, i.e., a required maximum error for the transducer of less than 5 mB in a temperature range from -50 to $+70$°C.

Most of the transducers offered could not meet the requirements due to significant zero and sensitivity shifts, nonlinearities, and fragile mechanical construction introducing considerable base strain effects.

Derivation of a Nonlinear Calibration Method

The well-known behavior of semiconductor strain gauges is that the resistance variation obeys a parabolic function of strain ϵ:

$$\frac{\Delta R}{R_0} = \left(\frac{T_{\text{ref}}}{T_0}\right) K\epsilon + \left(\frac{T_{\text{ref}}}{T_0}\right) K\epsilon^2 \tag{1}$$

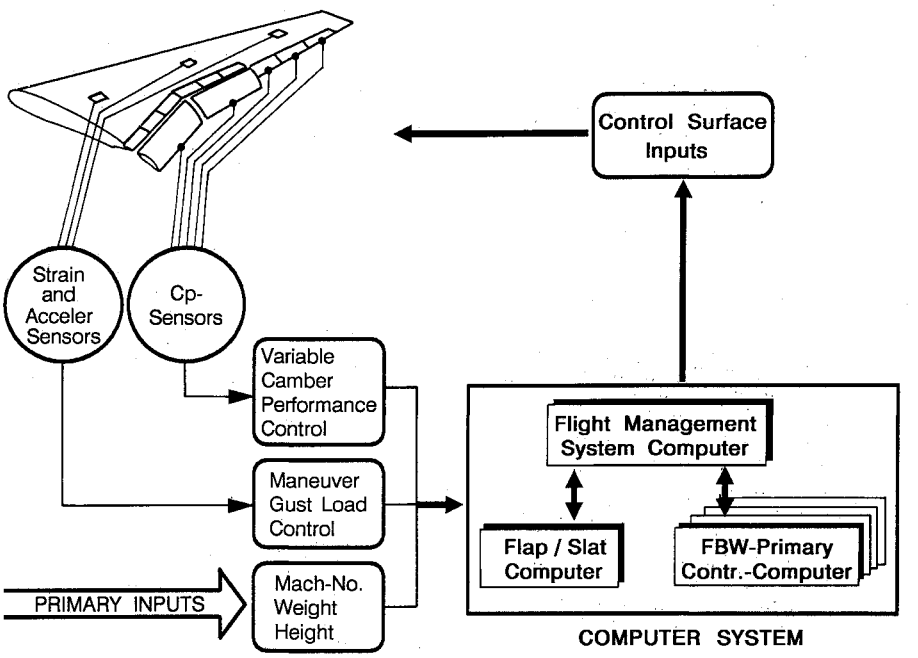

Fig. 1 Control system "intelligent wing."

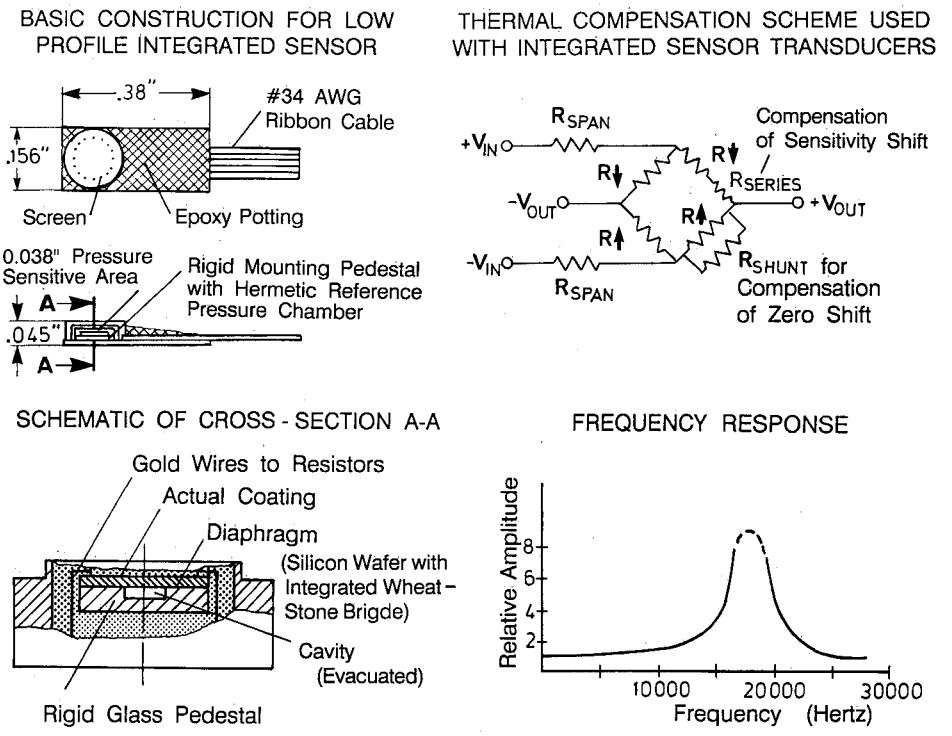

Fig. 2 Principle of piezoresistive transducer.[7]

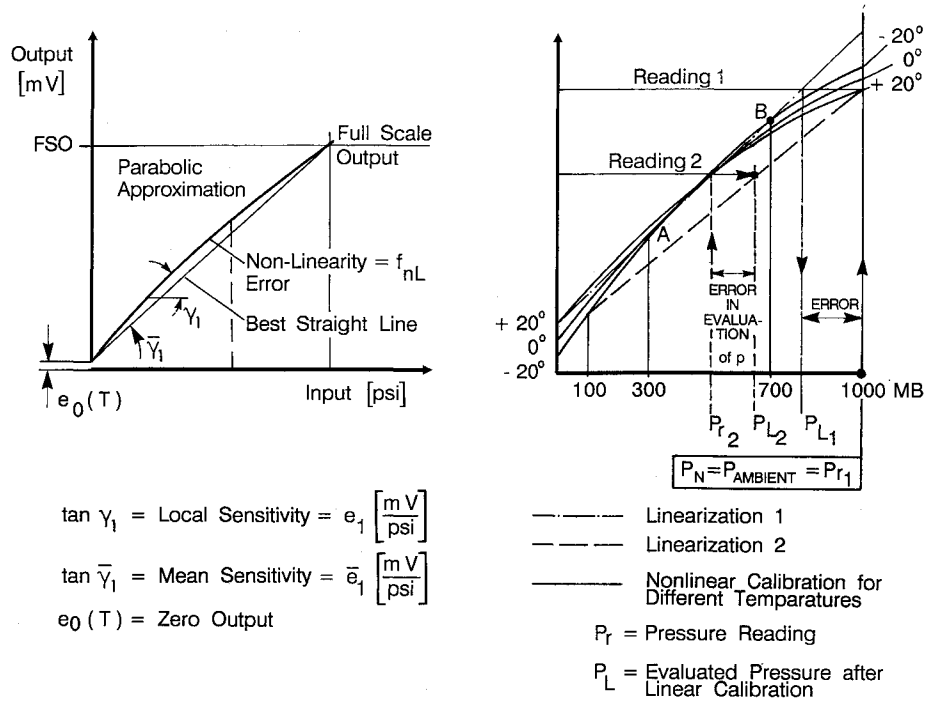

Fig. 3 Effect of linearization on evaluation of pressure.

where T denotes the temperature. This led to the formulation of a general nonlinear calibration function,

$$U(p,T) = a_{00} + a_{10}T + a_{20}T^2 + a_{30}T^3 + (b_0 + b_1T)\Delta p + (c_0 + c_1T)\Delta p^2[\text{mV}] \quad (2)$$

with $\Delta p = p - P_{\text{ref}}$, where P_{ref} is the reference ambient pressure. The constants are determined by a least-squares regression method. The zero output signal

$$e_0(T) = a_{00} + a_{10}T + a_{20}T^2 + a_{30}T^3 \text{ [mV]} \quad (3)$$

is usually approximated with a remaining error of typically less than 0.3% of full-scale output (FSO). The parabolic approximation of $U = f(p, T = \text{const})$ in Fig. 3 is accompanied by an error of less than 0.1% of full scale. In contrast to this procedure, the manufacturers usually guarantee maximum errors with respect to a linear regression or "best straight-line fit" (BSL fit). The nonlinearity error is then given by

$$f_{nL} = \max \{ |e_0(T) + b\Delta p + c\Delta p^2 - U_{\text{BSL}}| \} \quad (4)$$

Figure 3 shows that the term "sensitivity" is suitable only for the BSL fit and must be exchanged by "local sensitivity." This is given by

$$e_1 = \left.\frac{\partial U}{\partial p}\right|_{T=\text{const}} = b_0 + 2c_0p + \underbrace{(b_1 + 2c_1\Delta p)T}_{\text{sensitivity shift}} \quad (5)$$

The sensitivity shift due to deformation of the case, the base strain, was found to be larger than the thermal sensitivity shift.

The calibration coefficients are a function of excitation voltage only. Because cable resistance from the power supply to the transducer is nonnegligible, the coefficients were approximated further as a parabolic function of excitation. The shift in excitation is given by

$$\frac{\Delta U_{\text{ex}}}{U_{\text{ex}}} = \frac{1}{1 + R_{\text{trans}}/R_{\text{cable}}} \quad (6)$$

which is on the order of 10–15 mV for a typical installation. In normal application, the flight-test instrumentation engineer would apply a linear calibration with zero offset and a gain for the amplifier such that a BSL fit is achieved. Figure 3 shows two examples for such a setting. Linearization 1 reproduces the nonlinear characteristics in points A and B at − 20°C (with A and B equal to 300 and 700 mB, respectively), giving little error in flight conditions, whereas the ambient pressure is misread by ~200 mB. If setting 2 is selected, which reproduces the ambient pressure, the pressure is generally overestimated the lower the pressure and temperature readings. Hence, this could be avoided only by using a nonlinear calibration function.

Influence of Environment on Transducer Properties

In the flight-test environment, additional errors could be caused by moisture, icing, radiation, noise, vibration, and elastic deformation of the case.

Figure 4 shows the typical calibration results for a 15-psia absolute pressure transducer. The zero output is quite nonlinear, whereas the sensitivity is a linear function of pressure due to the base strain effect.

The coating on the first test transducers has been fairly thin, and, in several cases, even the connectors were uncovered. As a result of water drop impingement, a local electrolysis element was formed and the transducer was destroyed. Vibration and insufficient potting of the transducer cables caused a broken solder tack inside the transducers, and the shielding was not attached to the metal case for all test specimens, causing additional noise on the signals.

Since we were not satisfied with the first design, we investigated the influence of additional coatings as moisture protection. A transducer was provided with an additional silicon rubber coat and recalibrated. Figure 4 shows no dramatic influence. The sensitivity loss of 0.8% and the increase of nonlinearity by ~7% are acceptable, because they can be taken into account in the calibration function.

A significant influence of solar radiation was found when exposing the transducer to an ultraviolet lamp. A maximum shift of 1% FSO was measured, and, therefore, an opaque coating was requested to reduce the photo effect on the diffused resistors.

Consultations with the manufacturers led to design modifications of the prototypes, which were again tested in the laboratory. The modified transducers of two different compa-

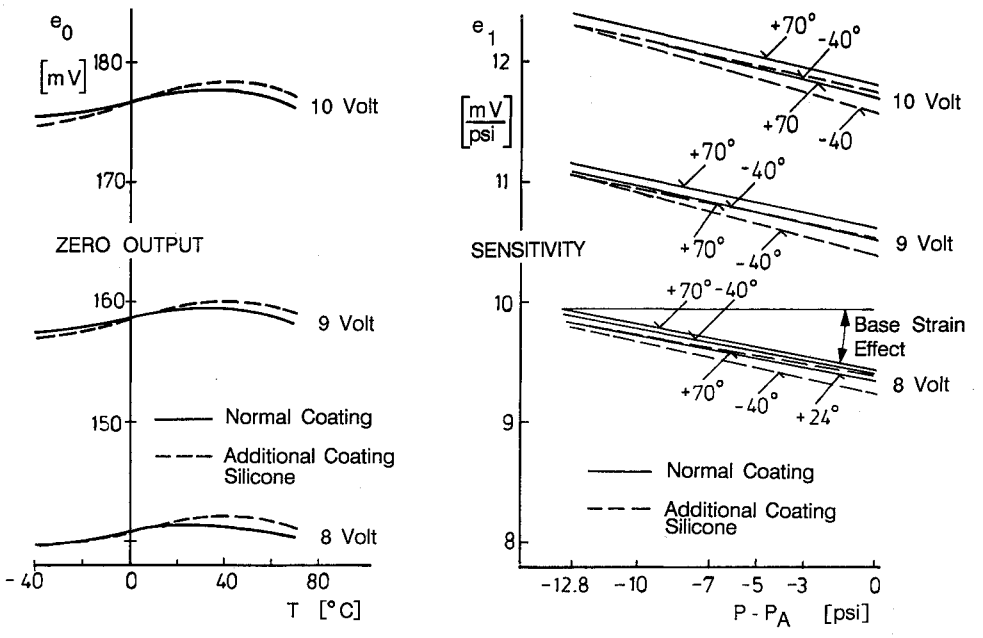

Fig. 4 Typical calibration results for an absolute pressure transducer.

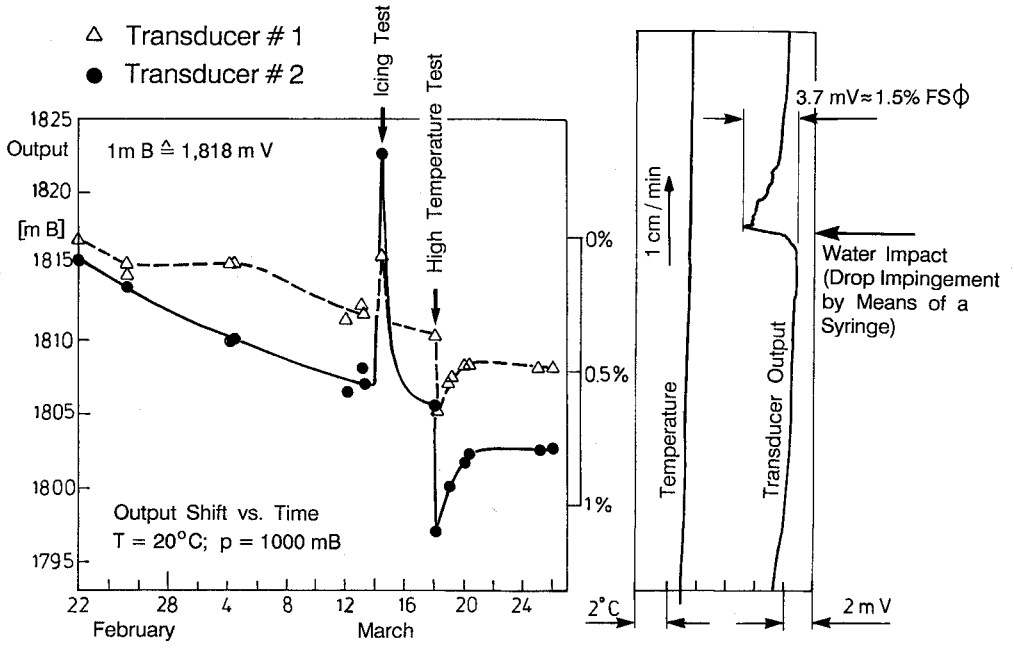

Fig. 5 Effects of moisture and icing on transducer output.

nies both had an M-screen above the pressure sensor, which was coated with parylene.

To simulate raindrop impingement during flight (especially important in the nose region of the wing), water was sprayed onto the screen using a syringe. The jet impinged the screen, and small droplets may have entered the cavity underneath the screen. The immediate reaction is shown on the right side of Fig. 5. An immediate deviation in output of 1.5% FSO was observed. After 8 min, the old value reestablished due to vaporization. Since raindrop impingement cannot be avoided during flight, this is not tolerable and several new design modifications were proposed.

The transducers exhibited an aging effect, too. After a few thermal cycles (ambient, −40°C, ambient, and so forth), an icing test, and a high-temperature shock, a decrease of sensitivity of 0.5% was found (Fig. 5). Therefore, the transducers should be "aged" before delivery by means of several temperature cycles.

In close cooperation with the transducer manufacturers, design modifications were proposed and realized. The results were two more rugged sensors with reduced errors.

Measurement of Trailing-Edge Pressures on an A310-200 at High Speeds

As a first application in flight, an experiment was defined to study the steady and unsteady trailing-edge pressures in the buffet onset (BO) regime of an A310-200 wing. The test arrangement in Fig. 6 shows the attachment to the thick trailing edge of the transonic wing with an aluminum rod at seven spanwise stations, which were chosen in correlation with an earlier flight-test aircraft with scanivalves.

The flight test on the A310-200 has shown maximum errors of ±5 mB, which in the high-speed regime is equivalent to $\Delta_p \approx \pm 0.05$. Stabilized flight-test points were flown with a stabilization of at least 30 s. Close to buffet boundary C_l variations were achieved by windup turns.

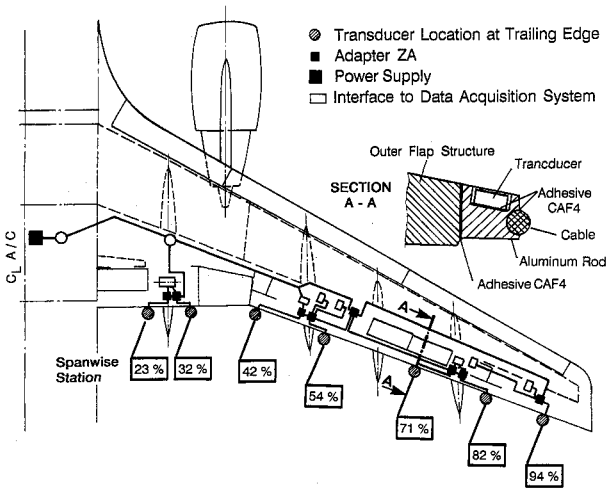

Fig. 6 Test arrangement on an A310 aircraft for high-speed test on trailing-edge pressures.

For a low Mach number of 0.73, Fig. 7 shows the spanwise development of trailing-edge pressure with increasing C_z, which seems reasonable compared with the wind-tunnel tests. Because there are strong three-dimensional effects in the trailing edge, the divergence of trailing-edge pressure was chosen for determination of BO and not the change in sign. A test close to the buffet boundary is depicted in Fig. 8. The pressure minimum at $\eta = 0.71$ indicates that high-speed stall and BO will occur initially at this station. The comparison with an earlier flight on a pressure-plotting aircraft is quite good, and the difference of 0.05 is within the error band. However, the spanwise development is in excellent agreement with the scanivalve results.

In flight, the operational buffet limit is determined by the pilot comfort sensation corresponding to the amplitude of the oscillation (0.2 g peak to peak) as measured by an accelerometer located underneath the pilot's seat. This measurement is obtained during a windup turn or a pitchup maneuver where the lift coefficient is increased progressively. The lift and incidence corresponding to the 0.2-g signal are denoted as the buffet limit (Fig. 9). This method does not take into account the structural transfer function between the aerodynamic action on the wing and the accelerometer output at the pilot seat.

The high-speed stall and BO of modern transonic wings are very close together; in fact, in Fig. 12 stall occurs ~ 1 s after the 0.2-g signal. It is obvious that these unsteady phenomena call for local flow measurement of the fluctuating pressures to achieve better physical understanding. Our present prediction method, based on the deviation of a steady lift-curve slope ($\Delta\alpha = 0.2$ deg) in a wind tunnel and the transposition to flight by using a reference method, is completely inadequate to predict the operational buffet limit, as the comparison of A300 and A310 illustrates.

Since we learned from Fig. 8 that separation starts at $\eta = 0.71$, the corresponding pressure transducer was taken for determination of BO in Fig. 10. The criterion was the divergence in c_p at the trailing edge. The linear calibration fails completely, but the nonlinear method agrees very well with the operational limit. For lower Mach numbers, the nonlinear increase is not reproduced. This could be correct, because the increase was measured with more forward c.g. locations.

For unsteady pressure evaluations, one of the main shortcomings of absolute pressure transducers, the zero shift, could be omitted and the pressure fluctuations will be measured quite accurately. The peak spectrum in Fig. 11 (peak mode, i.e., for a filter bandwidth of 0.5 Hz for each Δf, the peak rms value is plotted) exhibits excitation of structural modes of bending and torsion.

The harmonics of torsion can be detected up to the eighth order. Such an excitation indicates strong buffet motion. From airfoil measurements,[8] buffet can be divided into light and strong buffet. For light buffet, the spectrum does not exhibit distinct frequency peaks; i.e., it is more or less white noise. In the region of strong shocks and shock-induced separation, however, distinct peaks are observed as a result of the oscillating shock wave and periodic separations. According to Ref. 8, these buffet frequencies are 45–70 Hz for $M = 0.7$–0.78 for airfoils.

In three-dimensional flow, at flight conditions these frequencies are considerably lower. In addition to structural resonance, excitation of strong buffet was observed at $f_b = 16$ Hz and $M = 0.6$ and $f_b = 25$ Hz and $M = 0.73$. Higher harmonics of up to fourth order are detected (Fig. 11). The buffet boundary also could be derived from the divergence in the rms value of the pressure fluctuation. Since this is a more physical approach, it should give an improvement compared with the criterion of steady pressure divergence. In fact, there is an increasing difference in α_{BO} between both criteria (0.2 deg at $M = 0.6$; 0.7 deg at $M = 0.8$). That is, a shift to higher C_z values and toward the operational buffet boundary in Fig. 10.

Future predictions could be based on a higher-order reference method using not only the lift divergence but also unsteady pressure signals on wind-tunnel models for new and reference aircraft.

Measurement of Pressure Distribution and Boundary-Layer State in a High-Lift Configuration on an A310–300

Instrumentation and Flight-Test Program

In the context of a European research activity in the high-lift regime, a flight-test experiment devoted to pressure measurement and transition detection was performed recently. Detailed measurements of the boundary-layer flow in two and three dimensions on wind-tunnel models were obtained earlier with a maximum Reynolds number of 11×10^6 in the ONERA F1 wind tunnel on a A310 half model at 59% span. To close

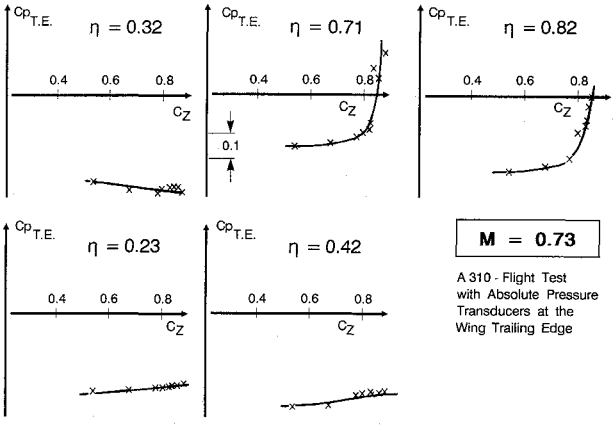

Fig. 7 Trailing-edge pressures vs lift.

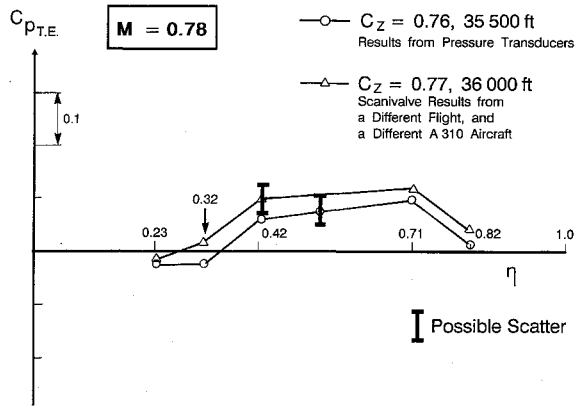

Fig. 8 Comparison of trailing-edge pressures vs span close to buffet boundary.

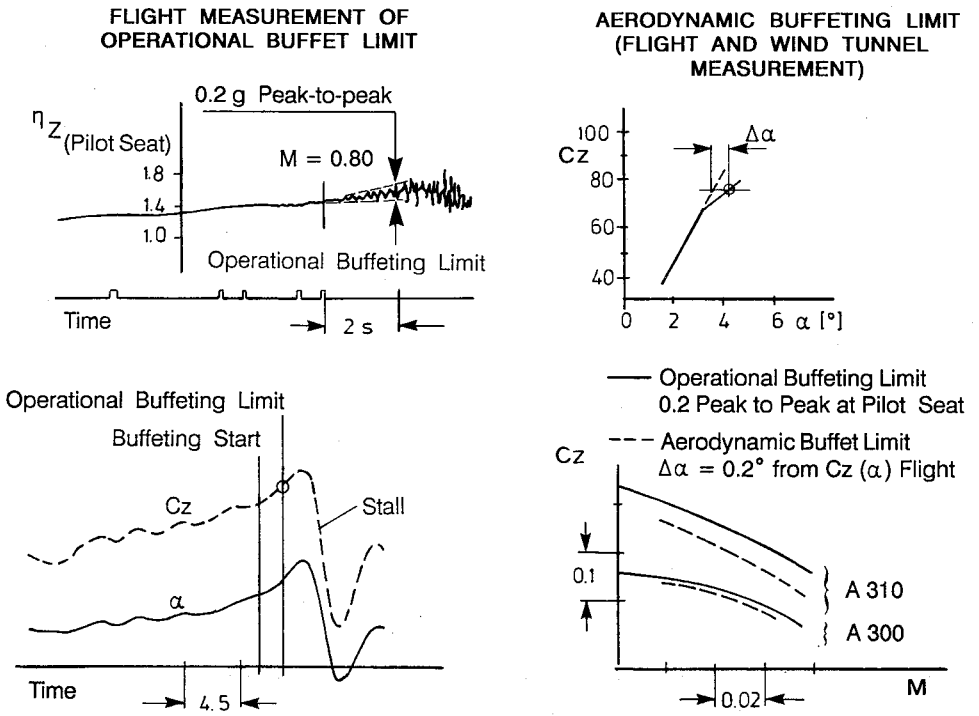

Fig. 9 Determination of buffet limits from flight tests and wind tunnel.

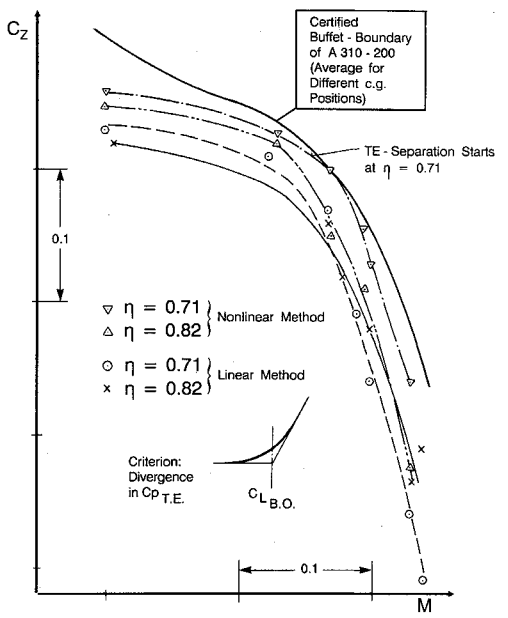

Fig. 10 Comparison of buffet limit from trailing-edge pressure with operational buffet limit.

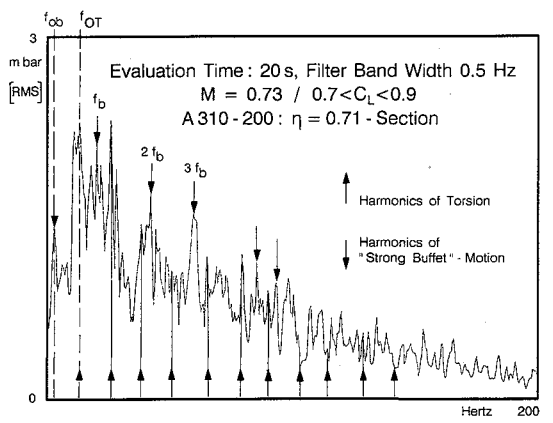

Fig. 11 Power spectrum of fluctuating pressures.

the gap in Reynolds number, a flight-test program was set up that required flights with low weights in high altitude at lifts close to minimum stall speed.

A representative section at 59% span was chosen for comparison with the wind tunnel models. Figure 12 gives an overview of the instrumentation. At spanwise station 59%, a complete pneumatic tubing within different plastic belts around the slat, wingbox, and flap with 70 pressure orifices was bonded onto the skin with an adhesive film. Slat 2 was covered totally with a belt to avoid large-scale disturbances propagating along the attachment line. Since there were predictions for a possible laminar attachment line in certain flight conditions, two rows of hot-film sensors at $\eta = 59$ and 64.5% were installed to detect transition. In between the hot films and the tubing, six absolute pressure transducers were bonded into a recess flush with the belt surface.

In addition, two boundary-layer rakes were installed: one at the slat trailing edge and the other at 50% local chord to validate the three-dimensional boundary-layer codes.

The flights were performed in a typical takeoff (slat 20 deg, flap 20 deg) and landing configuration (slat 30 deg, flap 40 deg). The envelopes in Figs. 13 and 14 show that Reynolds numbers close to the wind tunnel have been achieved, and the hatched regions denote that laminar flow regions have been observed on the slat. In these regions, additional sweeps with constant deceleration of 1 kt/s and steady sideslip flights were performed to investigate the transition process and the effect of leading-edge sweep.

Pressure Distributions

The agreement of the pressure distributions of the overlay tubing with the wind-tunnel results (Fig. 15) is generally good. A significant peak was measured in the wind tunnel and not in flight only in the region of the wingbox upper surface at $X/C = 0.2$. This is due to the slat trailing edge, which requires a surface slope change on the wingbox nose when it is stowed into retracted position. The glove over the wingbox creates a much smoother slope change as it is incorporated into the models. The suction peak on the slat, however, is more pronounced in the wind tunnel than in flight.

The comparison of slat pressures from the scanivalve and the transducers using the nonlinear calibration (Fig. 16) shows the same trend. Generally the agreement is fairly close, but the

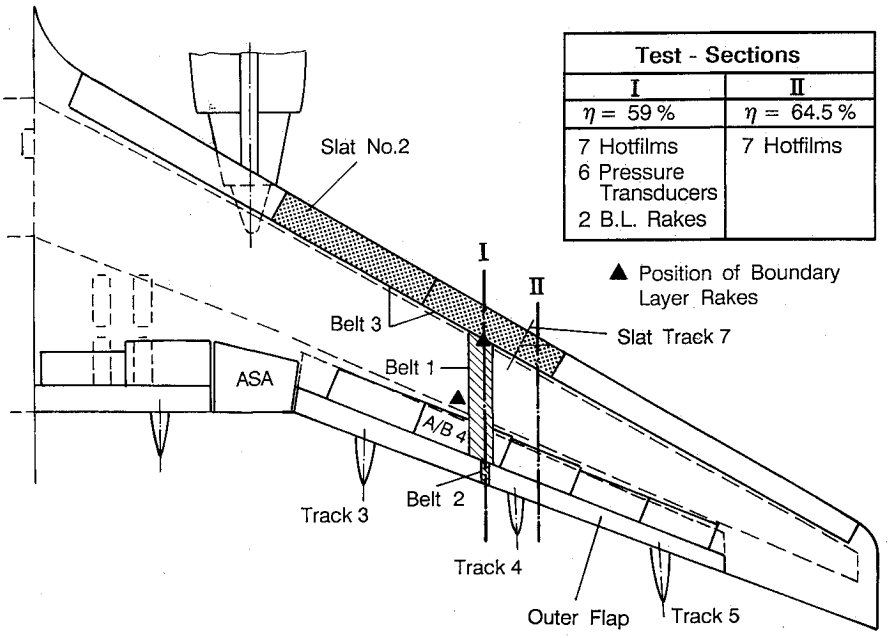

Fig. 12 General arrangement of high-lift experiment on an A310-300.

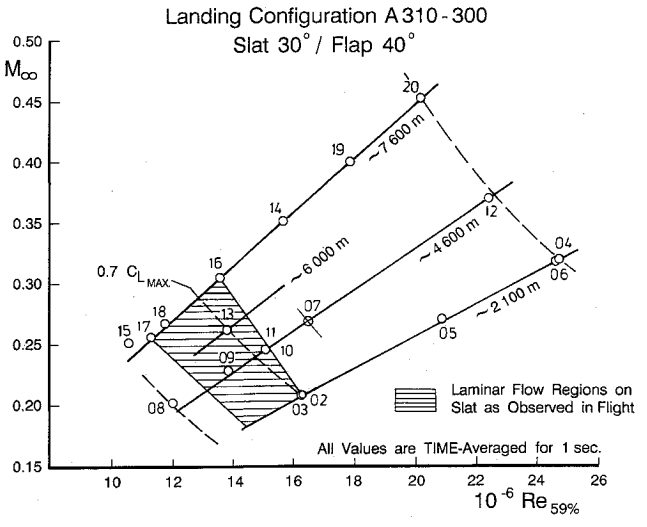

Fig. 13 Flight-test data points (landing).

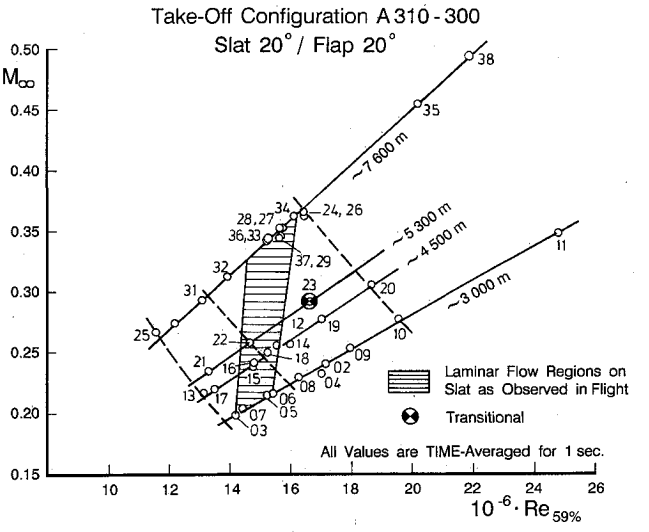

Fig. 14 Flight-test data points (takeoff).

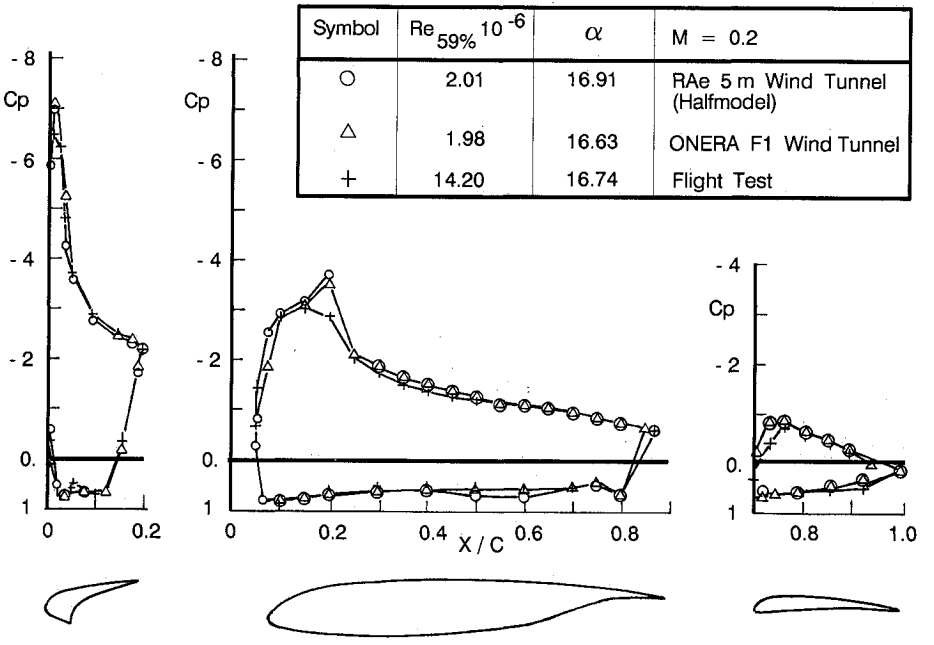

Fig. 15 Pressure distribution comparison—takeoff configuration.

suction peak from the transducers, especially at high lifts, is more pronounced. This seems reasonable because the time constant of the tubing with tube lengths of 5–10 m is up to 66 ms, which is much too long for a sampling sequence of 1 s for 24 scaniports, taking into account that a flight close to minimum stall speed is not very steady.

The modified transducer design worked well in flight test. Neither additional problems with humidity or icing nor long-term effects on transducer sensitivity were observed.

Investigation of Boundary-Layer State

Transition detection is based on the observation that fluctuating pressures or wall shear stresses rise to a peak value in the intermittent region, after which they drop to a fairly constant value in the turbulent boundary layer, which has a higher rms value than in the laminar flow region. Identification is not always easy, because there is usually a lot of noise superposed on the results. Figure 17 shows an example in the landing configuration. The hot films are located well around the complete slat nose, and some of the transducers are located in between the hot films.

From the pressure distributions, the position of the attachment line and the suction peak were determined. The attachment line and the complete leading edge were laminar. Shortly after the suction peak and before the slat hook, an intermittent state was detected. In Fig. 18, a sweep variation starting

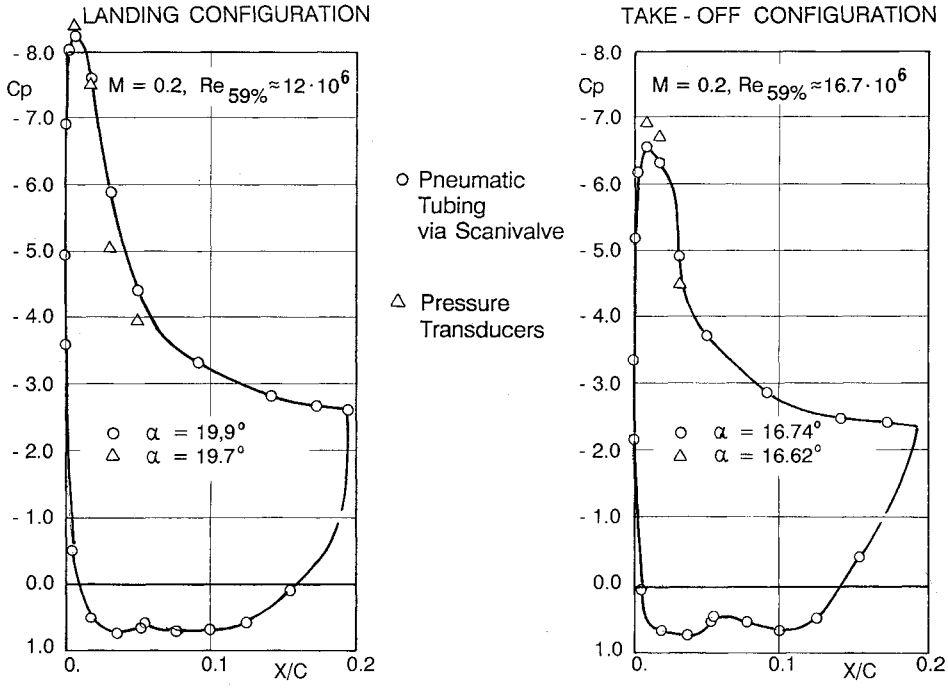

Fig. 16 Comparison of slat pressures with tubing and transducers.

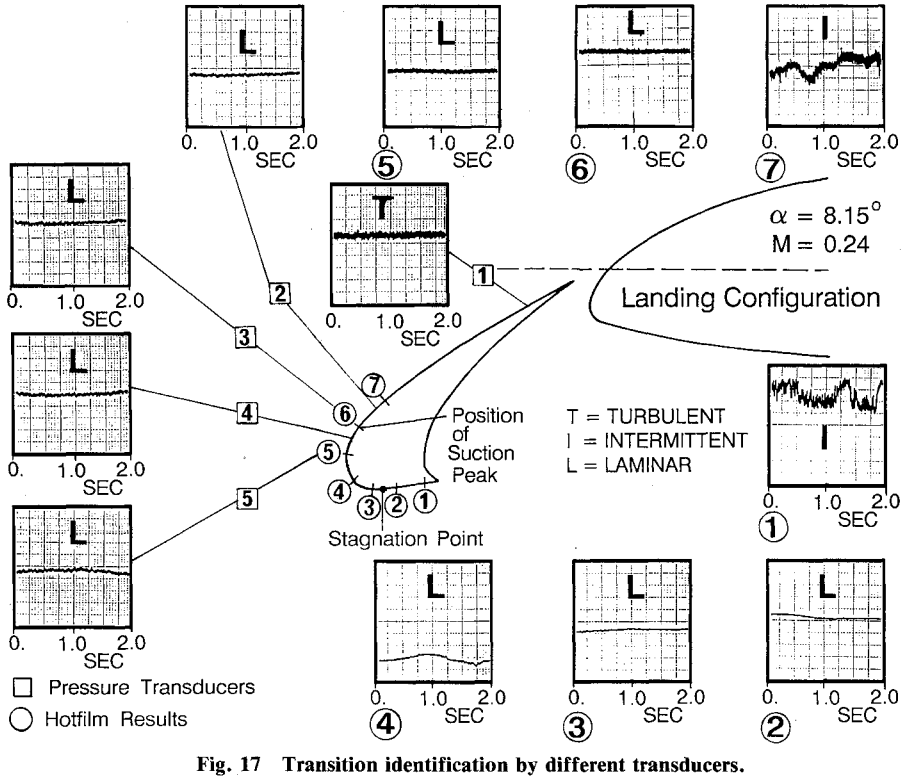

Fig. 17 Transition identification by different transducers.

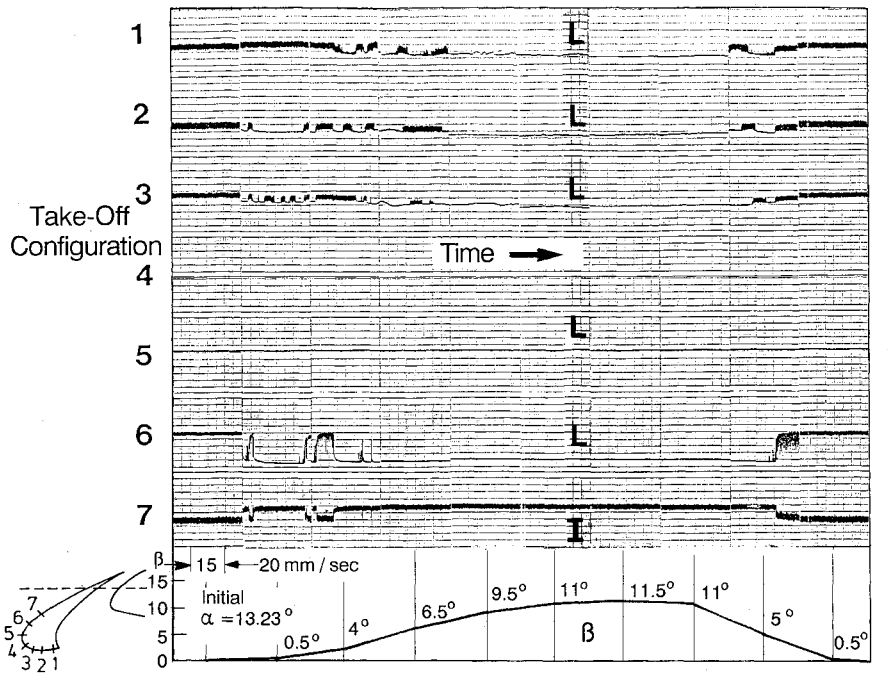

Fig. 18 Effect of a sweep variation on transition.

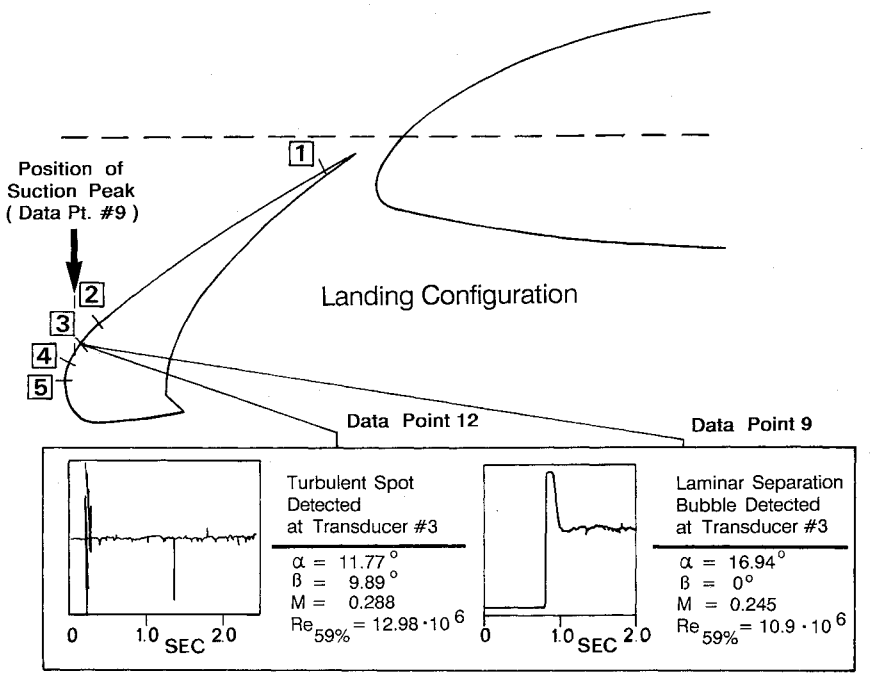

Fig. 19 Identification of boundary-layer state from pressure fluctuations.

from an initially turbulent state is depicted. At sideslip angles of 6 deg (i.e., a leading-edge sweep of 24 deg), a relaminarization occurs, whereas the transition back to turbulent flow is evoked at 4 deg (i.e., 26-deg sweep), showing some hysteresis effect.

Another example for the identification of the boundary-layer flow is given in Fig. 19. Turbulent spots in intermittent flow can be detected easily, and, in the case of data point 9, at nearly maximum lift and low Reynolds number a laminar separation bubble can be proven shortly after the position of the suction peak.

Changes in the state of the attachment-line flow should also be noticed in the boundary-layer profile at the slat trailing edge. Figure 20 compares the effect of a slight incidence increase of 1 deg in the pressure distribution, the hot-film signals close to the attachment line, and the total velocity profile at the trailing edge. The change from laminar to turbulent attachment-line flow corresponds with the thicker boundary layer. The same effect can be obtained by variation of the sweep angle.

For those data points where laminar attachment-line flow was found, the attachment-line Reynolds number $\bar{R}$ was computed as

$$\bar{R} = \sin\phi_{LE}\sqrt{\frac{Re_{59\%}}{U_1}} \tag{7}$$

where U_1 is the velocity gradient at the attachment line with respect to the arc of the airfoil according to Poll.[9] The results are given in Figs. 21 and 22 for both configurations.

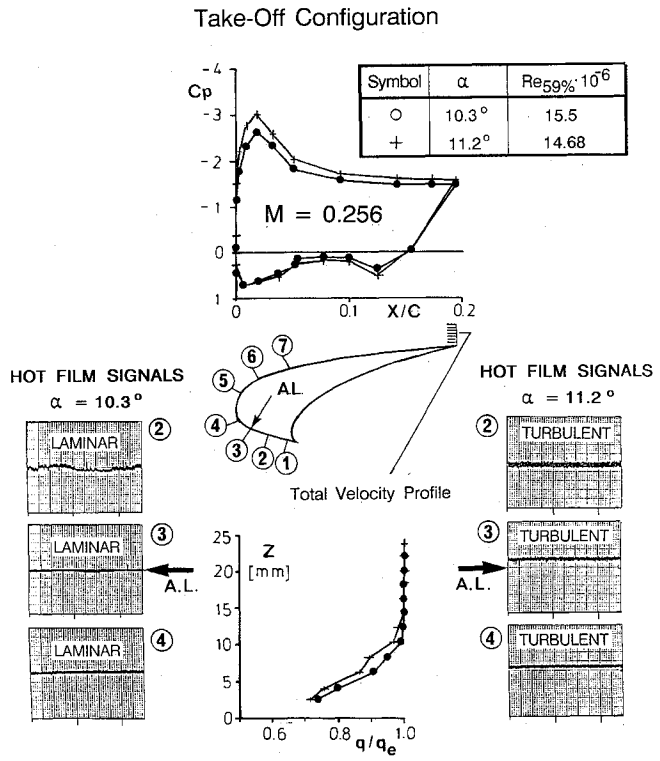

Fig. 20 Effect of incidence variation on boundary-layer properties.

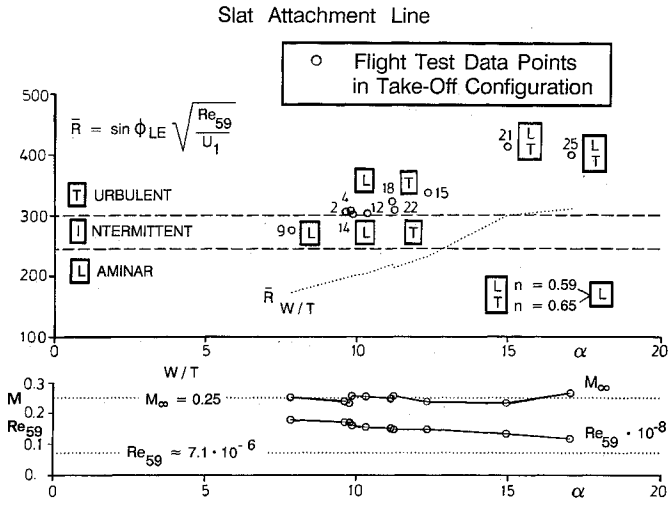

Fig. 21 Evaluation of Poll criterion for takeoff configuration.

According to Poll, transition is evoked due to a disturbance propagating along the attachment line at $\bar{R}>245$. For the takeoff case, this seems correct; however, for lowest Reynolds numbers, the laminar attachment line has been measured up to $\bar{R}=400$. For the landing case, laminar flow exists up to $\bar{R}\approx 300$.

The state of the attachment line seems to be very sensitive in the incidence region between 10 and 13 deg. Its position is always located between hot films 2 and 3 in a region of high curvature change. The resulting high $\bar{R}$ values up to 400 indicate that large disturbances do not cross that section in flight, which is rather unlikely in this configuration, or that the Poll criterion is too conservative. This gives rise to the assumption that attachment-line contamination for a laminar flow wing is less critical than expected concerning the design of natural laminar flow wings.

Conclusions

Absolute pressure transducers were investigated in laboratory and flight-test environments as a means to overcome the time-consuming and expensive installation of pneumatic tubings with their inherent error sources.

The flight-test environment is quite different from the laboratory conditions, and the available sensors do not yield acceptable accuracy. To cope with the large temperature range and environmental impact, a new transducer has been developed. The usual method of the "best straight-line fit" was found to be insufficient to describe the nonlinear behavior of silicon diaphragms. A nonlinear calibration function comprising the thermal, elastic, and cable influences was derived and proven in laboratory and wind tunnel tests. A preliminary flight test on an Airbus A310, where the trailing-edge pressure in high speed was investigated, has shown good agreement with former scanivalve tests. In addition, a derivation of the buffet boundary from the pressure fluctuation divergence was possible, which is a more physical approach than the usual accelerometer signal underneath the pilot seat.

In the context of a recent research flight-test experiment in the high-lift regime, the sensor signals were also used to determine transition from laminar to turbulent flow in comparison with hot-film sensors, which agreed very well. The static pressure distribution was compared with a scanivalve result from an overlay tubing; it was found to be in good agreement as well. From the pressure distributions and the detected boundary-layer state, a check of the Poll criterion for laminar attachment-line flow was derived. Laminar conditions were found well beyond the critical Poll number, $\bar{R}=245$. Hence, attachment-line contamination seems to be a less critical item for the design of laminar flow wings.

The transducer concept has been well proven as a viable alternative to traditional techniques. The pressure pickups can

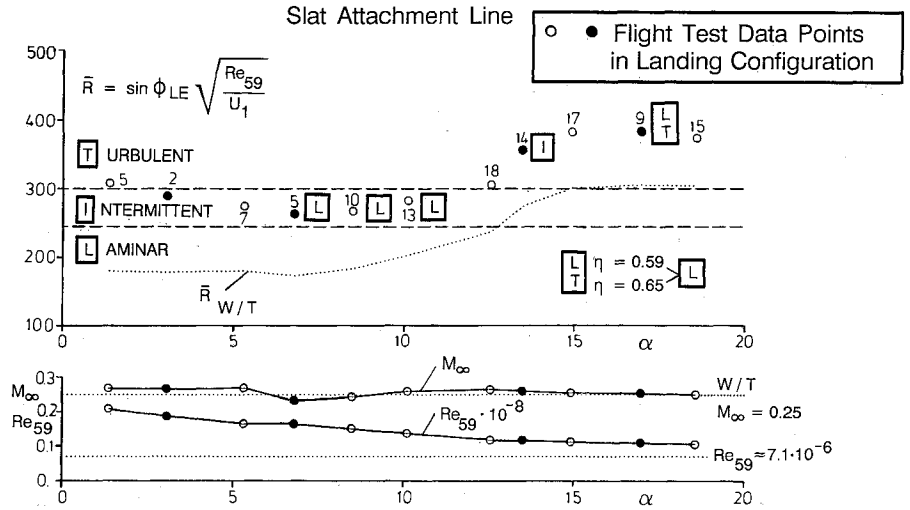

Fig. 22 Evaluation of Poll criterion for landing configuration.

be integrated in a plastic glove that is bonded to the wing at any desired location. Moreover, this system gives detailed information of the flow properties in unsteady flow, which is impossible for a scanivalve. Regarding the new technologies in the next-generation transport aircraft (i.e., load alleviation, *L/D*, and buffet control), which imply unsteady phenomena, such integrated sensor techniques are a prerequisite element in the control system of an intelligent transport aircraft wing.

References

[1]Whitmore, S., "Formulation of a General Technique for Predicting Pneumatic Attenuation Errors in Airborne Pressure Sensing Devices," AIAA Paper 88-2085, 1988.

[2]Ducruet, C., and Dyment, A., "The Pressure Hole Problem," *Journal of Fluid Mechanics,* Vol. 142, May 1984, pp. 251-267.

[3]Shaw, R., "The Influence of Hole Dimensions on Static Pressure Measurement," *Journal of Fluid Mechanics,* Vol. 7, April 1960, pp. 550-563.

[4]Bateman, L., "System Design Trends in Commercial Transport Aircraft," AIAA Paper 86-2722, 1986.

[5]Szodruch, J., "Variable Wing Camber for Transport Aircraft," *Progress in Aerospace Science,* Vol. 25, No. 3, 1988, pp. 297-328.

[6]Greff, E., "Aerodynamic Design and Integration of a Variable Camber Wing for a New Generation Long/Medium Range Aircraft," ICAS Paper 88-2.2.4, Sept. 1988.

[7]Mallon, J., "Integrated Sensors for Surface Pressure Measurements," *26th Annual ISA Instrumentation Symposium,* Instrumentation Society of America, May 1980.

[8]Lee, B. H. K., and Ohman, L. H., "Unsteady Pressures and Forces During Transonic Buffeting of a Supercritical Airfoil," *Journal of Aircraft,* Vol. 21, No. 6, 1984, pp. 439-444.

[9]Poll, D. I. A., "Some Observations of the Transition Process on the Windward Face of a Long Yawed Cylinder," *Journal of Fluid Mechanics,* Vol. 150, Jan. 1985, pp. 329-356.